Radiology Case Reports 16 (2021) 3766–3771

Available online at www.sciencedirect.com

ScienceDirect

journal homepage: www.elsevier.com/locate/radcr

Case Report

Alveolar soft part sarcoma of the orbit: A case report ☆,☆☆

Takeshi Oda, MD[a], Kazufumi Kikuchi, PhD,MD[a,], Osamu Togao, MD,PhD[b], Shingo Baba, MD,PhD[a], Masahiro Mizoguchi, MD,PhD[c], Mika Tanabe, MD,PhD[d], Mamoru Ito, MD,PhD[e], Hidetaka Yamamoto, MD,PhD[f], Kousei Ishigami, MD,PhD[a], Akio Hiwatashi, MD,PhD[a]*

[a] *Departments of Clinical Radiology, Graduate School of Medical Sciences Kyushu University, Fukuoka, Japan*
[b] *Department of Molecular Imaging & Diagnosis, Graduate School of Medical Sciences, Kyushu University, Fukuoka, Japan*
[c] *Department of Neurosurgery, Graduate School of Medical Sciences, Kyushu University, Fukuoka, Japan*
[d] *Department of Ophthalmology, Graduate School of Medical Sciences, Kyushu University, Fukuoka, Japan*
[e] *Department of Hematology, Oncology and Cardiovascular Medicine, Kyushu University Hospital, Fukuoka, Japan*
[f] *Department of Anatomic Pathology, Graduate School of Medical Sciences, Kyushu University, Fukuoka, Japan*

ARTICLE INFO

Article history:
Received 24 August 2021
Revised 30 August 2021
Accepted 4 September 2021

Keywords:
Alveolar Soft Part Sarcoma
Magnetic Resonance Imaging
Fluorodeoxyglucose-Position Emission Tomography/Computed Tomography
Intraorbital Tumor
Flow Voids
Apparent Diffusion Coefficient

ABSTRACT

Alveolar soft part sarcoma is a rare soft tissue neoplasm that accounts for approximately 1% of all sarcomas and is usually identified in the extremities in adults. The occurrence of alveolar soft part sarcoma in the orbit is extremely rare, estimated at approximately 5% – 15% among all cases of alveolar soft part sarcoma . Here, we present a case of 29-year-old woman with orbital alveolar soft part sarcoma. We describe the magnetic resonance and F-18 2-fluoro-2-deoxy-D-glucose-position emission tomography/computed tomography findings of this case. This young woman had a spindle-shaped mass. A higher signal compared to the extraocular muscle on T1-weighted images, numerous flow voids on T2-weighted images, and intense enhancement could be key findings of this disease.

☆ Competing interests: The authors certify that there is no conflict of interest with any financial organization regarding the material discussed in the manuscript.

☆☆ Funding: This work was supported by The Shin-Nihon Foundation of Advanced Medical Research.

* Corresponding author.
E-mail address: kikuchi.kazufumi.953@m.kyushu-u.ac.jp (K. Kikuchi).

https://doi.org/10.1016/j.radcr.2021.09.005

Fig. 1 – Non-contrast axial CT reveals a spindle-shaped mass in the left orbit. There is no calcification in the mass (a) After contrast administration, a homogeneous enhancement is observed (b) Bone window CT (window level/width, 700/2000 HU) reveals thinning of the lateral wall (c; arrow). CT, computed tomography.

Introduction

Alveolar soft part sarcoma (ASPS) is a rare soft tissue neoplasm that accounts for approximately 1% of all sarcomas [1], and is usually identified in the extremities in adults or in the head and neck region in children [2]. Orbital ASPS is estimated to be approximately 5%-15% of all cases of ASPS [3,4], with a slight female predilection [2]. The extraconal regions are affected in approximately 89% of cases and intraconal regions are affected in about 11% of cases [5]. The median age of 13.5 years [6].

Herein, we report the case of a patient with orbital ASPS. We aimed to discuss the magnetic resonance imaging (MRI) including diffusion-weighted imaging (DWI) and F-18 2-fluoro-2-deoxy-D-glucose-positron emission tomography/computed tomography (FDG-PET/CT) findings associated with this case of orbital ASPS.

Case report

A 29-year-old Asian woman who was previously healthy presented to our hospital for complaining of discomfort, pain, and diplopia in her left eye lasting for one month. There were no significant medical or surgical histories and her family history showed that only her maternal aunt had colon cancer. Routine laboratory test results were normal. Physical examination revealed an exophthalmos in the left orbit and there were slight abduction and supination abnormalities of the left eye, which caused the eye position to be left inferior strabismus.

Computed tomography (CT) revealed a spindle-shaped mass with a well-defined border and smooth margin in the left orbit (Fig. 1). No calcification was observed in the mass (Fig. 1a). The mass showed an intense contrast enhancement (Fig. 1b). The lateral wall of the left orbit was slightly thinned by the mass (Fig. 1c).

MRI identified a 34 × 19 × 20-mm homogeneously enhancing spindle-shaped mass on the lateral side of the left orbit (Fig. 2), which extended to the superior orbital fissure. The location of the mass occupied both the intra- and extra-conal regions. The mass showed mildly high-intensity on T1-weighted images (T1WI) (Fig. 2a) and homogeneous high intensity on fat-suppressed T2-weighted images (T2WI) (Fig. 2c) compared to those in the medial rectus muscle. The left optic nerve and lacrimal gland were shifted by the mass without abnormal signal intensity. Many flow voids were observed within the mass on T2WI (Fig. 2c). On turbo-spin echo diffusion-weighted imaging (TSE-DWI) with $b = 800$ s/mm^2, the mass showed mild high intensity compared to that in the medial rectus muscle (Fig. 2d). The minimum apparent diffusion coefficient (ADC) of the solid area was 1.3×10^{-3} mm^2/s (Fig. 2e). The margin between the mass and the lateral rectus muscle was obscured (Fig. 2f), which implied its origin. A dynamic study revealed that the mass showed early and persistent enhancement (Figs. 2g).

FDG-PET/CT showed a mild FDG uptake. The maximum FDG uptake of the standardized uptake value (SUV) of the solid area was 3.2 (Fig. 3).

A solitary fibrous tumor, perivascular epithelioid cell tumor (PEComa) paraganglioma, meningioma, rhabdomyosarcoma, hypervascular metastatic tumor (eg, renal cell carcinoma), cavernous malformation (hemangioma), and schwannoma were all considered as differential diagnoses.

Surgical resection was performed via transcranial approach. The origin of the mass was identified as the lateral rectus muscle, and the lacrimal gland was intact based on intraoperative findings. The deep part of the mass at the apex of the orbit was not resected to preserve eye function.

Histopathological findings, hematoxylin and eosin (H&E) staining revealed that the tumor cells showed a nested growth pattern and were separated by fibrous trabeculae into well-defined nests of uniformly large, round-to-polygonal cells, surrounded by delicate sinusoidal vascular channels lined by a flattened, single layer of endothelial cells (Fig. 4a). The cytoplasm had an abundant granular, eosinophilic, and glycogen-rich appearance. Periodic acid–Schiff (PAS) staining showed intracytoplasmic glycogen and characteristic PAS-positive, diastase-resistant rhomboid or rod-shaped crystals were present (Fig. 4b). Immunohistochemistry revealed positive staining for an antibody that detects the carboxyl terminal portion of transcription factor E3 (TFE3) retained in the fusion protein (Fig. 4c), but negative staining for human melanoma black (HMB-45), which is associated with PEComa (Fig. 4d). In genetic analysis, ASPSCR1-TFE3 fusion was detected by RT-PCR and direct sequence. In conjunction with the histological

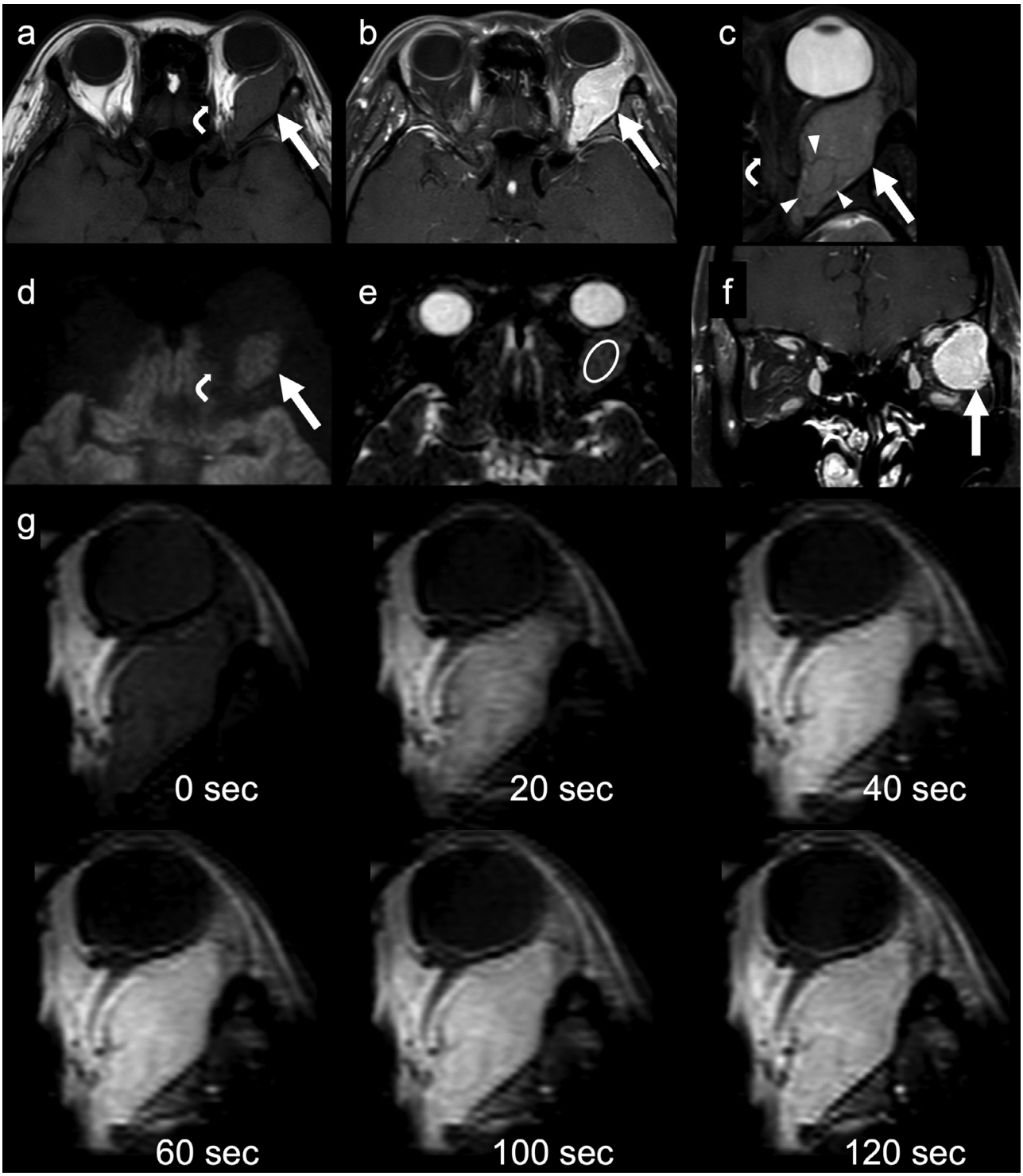

Fig. 2 – A spindle-shaped mass (arrow) in the left orbit with mildly high-intensity compared to that in the medial rectus muscle (curved arrow) is observed on non-contrast axial T1WI (a) On contrast-enhanced axial fat-suppressed T1WI, the mass shows homogeneous intense enhancement (b; arrow). On fat-suppressed T2WI, the mass (arrow) shows a high signal intensity compared to that in the medial rectus muscle (curved arrow) and many flow voids (arrowheads) are seen within the mass (c) On TSE-DWI with b = 800 s/mm^2, the mass (arrow) shows mild high intensity compared to that in the medial rectus muscle (curved arrow) (d). The ADC value of the solid area is 1.3 x 10^{-3} mm^2/s (e; ellipsoid). On contrast-enhanced coronal fat-suppressed T1WI, the margin between the mass and the lateral rectus muscle is obscured (f; arrow). A dynamic study shows early and persistent enhancements of the mass (g; 0 to 120 seconds) (G). ADC, apparent diffusion coefficient; DWI, diffusion-weighted imaging; T1WI, T1-weighted imaging; T2WI, T2-weighted imaging; TSE, turbo spin echo.

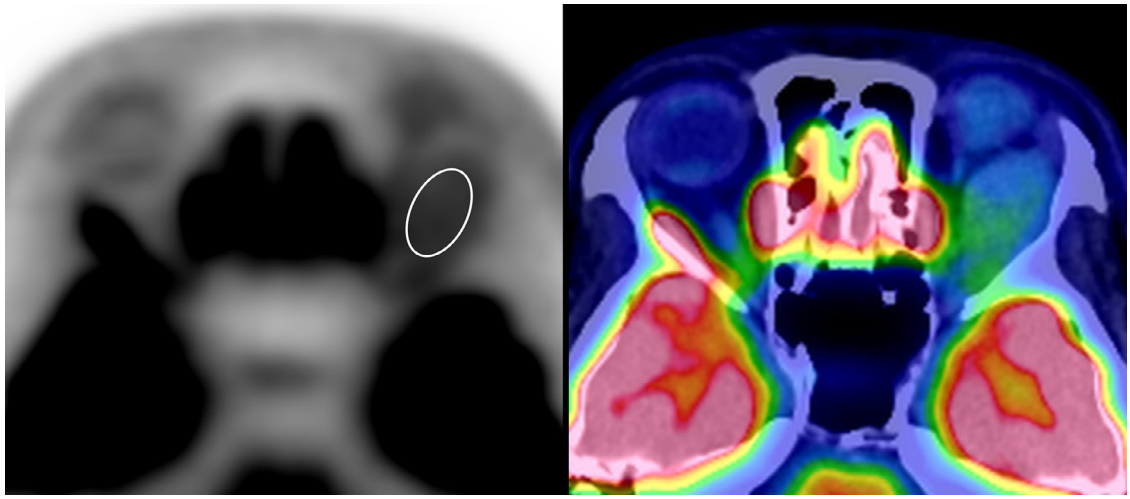

Fig. 3 – A spindle-shaped mass in the left orbit shows mild FDG uptake on FDG-PET/CT. The maximum FDG uptake of SUV of the solid area is 3.2 (ellipsoid). CT, computed tomography; FDG, F-18 2-fluoro-2-deoxy-D-glucose; PET, position emission tomography; SUV, standardized uptake value.

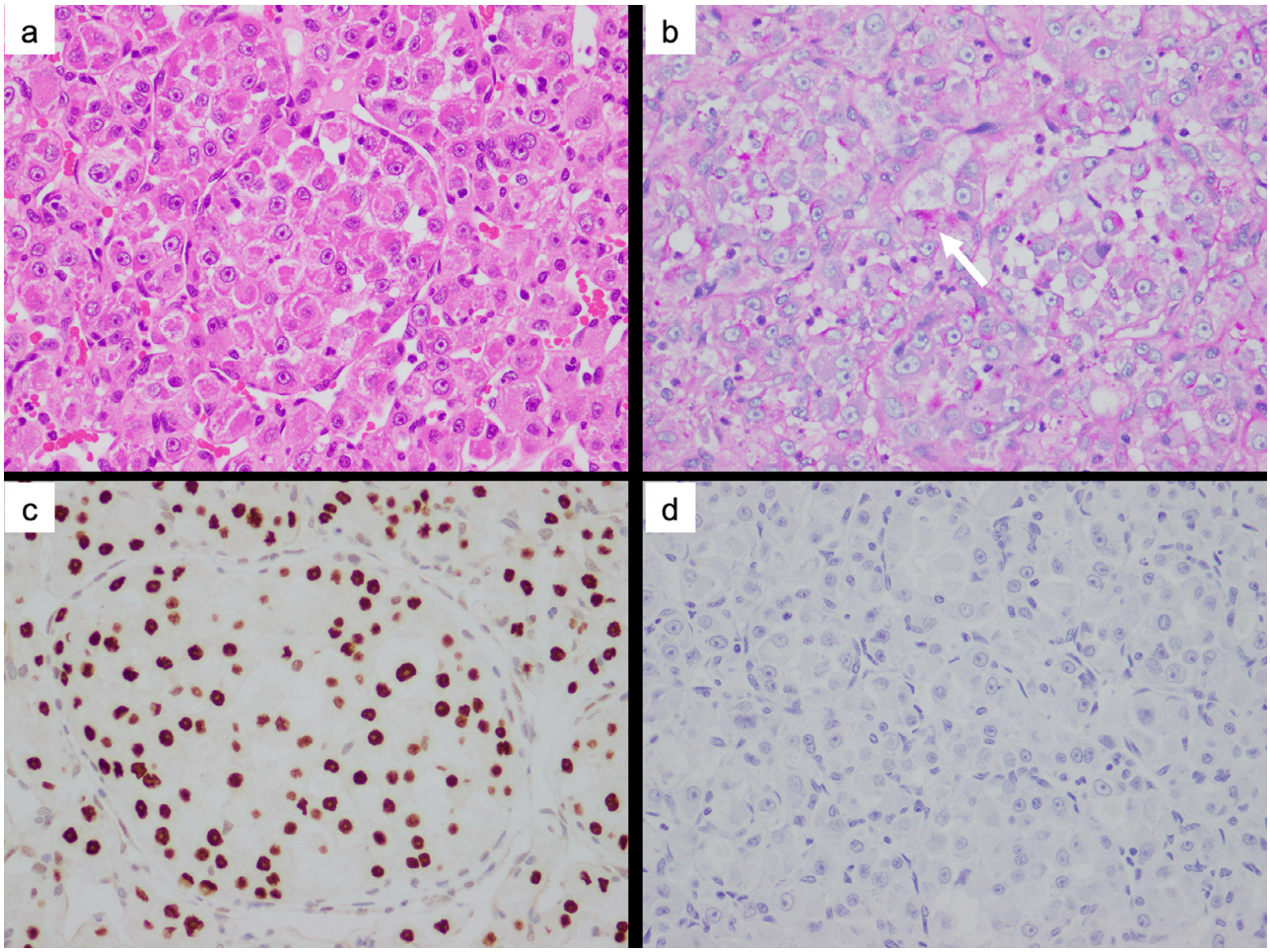

Fig. 4 – H&E staining of a section of the tumor shows a nested growth pattern separated by fibrous trabeculae into well-defined nests of uniformly large, round-to-polygonal cells, surrounded by delicate sinusoidal vascular channels lined by a flattened, single layer of endothelial cells (a). PAS staining section shows intracytoplasmic glycogen and characteristic PAS-positive, diastase-resistant rhomboid or rod-shaped crystals (b; arrow). On immunohistochemistry, the TFE3 region retained in the fusion protein (c) is positive, but negative for HMB-45 (d). H&E, hematoxylin and eosin; HMB-45, human melanoma black; PAS, periodic acid–Schiff; TFE3, transcription factor E3.

and immunohistochemical findings as well as genetic analysis, the mass was diagnosed as an orbital ASPS.

Discussion

ASPS was first defined and named by Christopherson et al. in 1952 [7]. This sarcoma type is highly vascularized with small vascular spaces separating nests of cells [8,9], and is characterized by a specific chromosomal alteration, der(17) t(X:17)(p11:q25), resulting in the fusion of the TFE3 transcription factor gene (from Xp11) with the alveolar soft part sarcoma critical region 1 (ASPSCR1), also known as alveolar soft part sarcoma locus (ASPL) at 17q25 [9]. ASPS is a rare, distinctive soft tissue sarcoma subtype, representing less than 1% of all soft tissue sarcomas [10]. In adults, ASPS tends to involve deep soft tissues in the thigh or buttocks. In children and infants, ASPS has a predilection for the head and neck region, with the tongue and orbit being the most common sites [11]. It tends to occur between the ages of 15 and 35 years, and is rare in patients younger than 5 years and older than 50 years [11]. It is more common in females than in males in a 2:1 ratio [9]. Based on a review of 172 cases, orbital ASPS is the second highest (15.1%) of all ASPSs [4].

Orbital ASPS presents a well-circumscribed, spindle-shaped mass that tends to intensify to moderate enhancement with enlarged vessels [2,3,12]. This appearance sometimes mimics a hemangioma [3,12].

On CT, orbital ASPS appears as an iso-dense mass compared to an extraocular muscle without calcification [3]. In our case, there was no destructive bone lesion in the orbital wall, but there was thinning of the lateral wall, suggesting pressure from prolonged gradual growth of the mass.

On MRI, orbital ASPS shows iso- to mildly high-intensity on T1WI and high-intensity on T2WI compared to an extraocular muscle. A previous pathological study reveals that ASPS showed intratumor hemorrhage [9]. Histopathological finding of our case, intratumoral hemorrhage was not evident; however, the high signal intensity on T1WI was presumably due to the hemorrhagic component. The presence of many flow voids on T2WI is a characteristic finding of this sarcoma reported in previous reports [3,13,14]. On post-contrast images, orbital ASPS has shown homogeneous intense enhancement [3,13,14]. These MRI findings were consistent with those of our patient.

A dynamic study showed that orbital ASPS in our patient had early and persistent enhancement. In previous studies, ASPS presented with numerous enlarged vessels with arteriovenous shunting in the arterial phase followed by intense tumor staining. Despite the rapid shunting of blood, the washout of contrast material from the lesion was slow [14-16]. These angiographic findings are consistent with those of the dynamic MRI study in this patient.

The minimum ADC of this sarcoma in the present case was slightly high (1.3×10^{-3} mm^2/s). To the best of our knowledge, there is no previous report regarding ADC derived from DWI in orbital ASPS. We speculate this is because of the technical difficulty in evaluating intraorbital structures with echo planar imaging, which is the most common imaging technique for DWI [17]. To solve this technical problem, the TSE-DWI technique has been proposed for orbital [17,18] and lung [19] regions. In a previous report, the ADC calculated in cases where ASPS is located in other body parts is $1.08 – 1.26 \times 10^{-3}$ mm^2/s on a 1.5-tesla MRI scanner [20]. The ADC of the sarcoma in the present case was slightly higher than those of previous cases [20], which could be because the orbital ASPS in the present case showed many flow voids on T2WI and elevated blood flow fraction, thus increasing the ADC derived from DWI [21].

In our patient, FDG-PET/CT showed mild FDG uptake. To the best of our knowledge, there are no previous reports regarding FDG uptake in a case of orbital ASPS. The maximum FDG uptake of SUV in patients with ASPS in other body parts is 1.8 – 10.1 [22-25]. A previous study reported the presence of thrombosed tumor vessels [3]. Because thrombosis induces inflammation, this wide range of FDG uptake may reflect the degree of intratumoral inflammation.

Conclusion

In conclusion, we report a case of orbital ASPS in a 29-year-old Asian woman. A spindle-shaped mass in the orbital region with a higher signal than the extraocular muscle on T1WI, numerous flow voids on T2WI, and intense enhancement could be key findings to differentiate orbital ASPS from other intraorbital tumor types.

Patient consent

The patient provided consent for publication of our case report.

REFERENCES

[1] Rose AM, Kabiru J, Rose GE. Alveolar soft-part sarcoma of the orbit. Afr J Paediatr Surg 2011;8:82–4. doi:10.4103/0189-6725.78936.
[2] Hei Y, Kang L, Yang X, Wang Y, Lu X, Li Y, et al. Orbital alveolar soft part sarcoma: a report of 8 cases and review of the literature. Oncol Lett 2018;15:304–14. doi:10.3892/ol.2017.7286.
[3] McCarville MB, Muzzafar S, Kao SC, Coffin CM, Parham DM, Anderson JR, et al. Imaging features of alveolar soft-part sarcoma: a report from children's oncology group study ARST0332. AJR Am J Roentgenol 2014;203:1345–52. doi:10.2214/AJR.14.12462.
[4] Ordóñez NG. Alveolar soft part sarcoma: a review and update. Adv Anat Pathol 1999;6:125–39. doi:10.1097/00125480-199905000-00001.
[5] Mulay K, Ali MJ, Honavar SG, Reddy VA, et al. Orbital alveolar soft-part sarcoma: clinico-pathological profiles, management and outcomes. J Cancer Res Ther 2014;10:294–8. doi:10.4103/0973-1482.136570.
[6] de Barros GF, Hakim JR, Passos JP, Perron M, Odashiro AN, et al. Orbital alveolar soft part sarcoma: case report and literature review. Can J Ophthalmol 2019;54:e292–4. doi:10.1016/j.jcjo.2019.02.005.

[7] Christopherson WM, Foote FW, Stewart FW. Alveolar soft-part sarcomas; structurally characteristic tumors of uncertain histogenesis. Cancer 1952;5:100–11. doi:10.1002/1097-0142(195201)5.
[8] Zarrin-Khameh N, Kaye KS. Alveolar soft part sarcoma. Arch Pathol Lab Med 2007;131:488–91. doi:10.5858/2007-131-488-ASPS.
[9] Jaber OI, Kirby PA. Alveolar soft part sarcoma. Arch Pathol Lab Med 2015;139:1459–62. doi:10.5858/arpa.2014-0385-RS.
[10] Paoluzzi L, Maki RG. Diagnosis, prognosis, and treatment of alveolar soft-part sarcoma: a review. JAMA Oncol 2019;5:254–60. doi:10.1001/jamaoncol.2018.4490.
[11] Fletcher CDM. World health organization, international agency for research on cancer. WHO classification of tumours of soft tissue and bone, Lyon: IARC Press; 2013. 4th ed.
[12] Chu WC, Howard RG, Roebuck DJ, Chik KW, Li CK, et al. Periorbital alveolar soft part sarcoma with radiologic features mimicking haemangioma. Med Pediatr Oncol 2003;41:145–6. doi:10.1002/mpo.10037.
[13] Itani M, Shabb NS, Haidar R, Khoury NJ, et al. AIRP best cases in radiologic-pathologic correlation: alveolar soft-part sarcoma. Radio Graphics 2013;33:585–93. doi:10.1148/rg.332115173.
[14] Suh JS, Cho J, Lee SH, Shin KH, Yang WI, Lee JH, et al. Alveolar soft part sarcoma: MR and angiographic findings. Skeletal Radiol 2000;29:680–9. doi:10.1007/s002560000285.
[15] Aiken AH, Stone JA. Alveolar soft-part sarcoma of the tongue. AJNR Am J Neuroradiol 2003;24:1156–8.
[16] Lorigan JG, O'Keeffe FN, Evans HL, Wallace S, et al. The radiologic manifestations of alveolar soft-part sarcoma. AJR Am J Roentgenol 1989;153:335–9. doi:10.2214/ajr.153.2.335.
[17] Hiwatashi A, Yoshiura T, Togao O, Yamashita K, Kikuchi K, Fujita Y, et al. Diffusivity of intraorbital lymphoma vs IgG4-related DISEASE: 3D turbo field echo with diffusion-sensitised driven-equilibrium preparation technique. Eur Radiol 2014;24:581–6. doi:10.1007/s00330-013-3058-9.
[18] Hiwatashi A, Togao O, Yamashita K, Kikuchi K, Kamei R, Yoshikawa H, et al. Diffusivity of intraorbital lymphoma vs inflammation: comparison of single shot turbo spin echo and multishot echo planar imaging techniques. Eur Radiol 2018;28:325–30. doi:10.1007/s00330-017-4995-5.
[19] Tyagi N, Cloutier M, Zakian K, Deasy JO, Hunt M, Rimner A, et al. Diffusion-weighted MRI of the lung at 3T evaluated using echo-planar-based and single-shot turbo spin-echo-based acquisition techniques for radiotherapy applications. J Appl Clin Med Phys 2019;20:284–92. doi:10.1002/acm2.12493.
[20] Cui JF, Chen HS, Hao DP, Liu JH, Hou F, Xu WJ, et al. Magnetic resonance features and characteristic vascular pattern of alveolar soft-part sarcoma. Oncol Res Treat 2017;40:580–5. doi:10.1159/000477443.
[21] Le Bihan D, Breton E, Lallemand D, Aubin ML, Vignaud J, Laval-Jeantet M, et al. Separation of diffusion and perfusion in intravoxel incoherent motion MR imaging. Radiology 1988;168:497–505. doi:10.1148/radiology.168.2.3393671.
[22] Montgomery JR, Conrad GR, Sinha P, Absher K, et al. FDG PET of alveolar soft part sarcoma. Clin Nucl Med 2010;35:827–9. doi:10.1097/RLU.0b013e3181ef0b57.
[23] Dong A, Wang Y, Cheng C, Zuo C, et al. CT, MRI, and FDG PET/CT in a patient with alveolar soft part sarcoma. Clin Nucl Med 2014;39:265–7. doi:10.1097/RLU.0b013e3182817b09.
[24] Wu ZJ, Bian TT, Zhan XH, Dong C, Wang YL, Xu WJ, et al. Computed tomography, magnetic resonance imaging, and F-deoxyglucose positron emission computed tomography/computed tomography findings of alveolar soft part sarcoma with calcification in the thigh: a case report. World J Clin Cases 2020;8:3349–54. doi:10.12998/wjcc.v8.i15.3349.
[25] Sood S, Baheti AD, Shinagare AB, Jagannathan JP, Hornick JL, Ramaiya NH, et al. Imaging features of primary and metastatic alveolar soft part sarcoma: single institute experience in 25 patients. Br J Radiol 2014;87:20130719. doi:10.1259/bjr.20130719.